Chinese Chemical Letters 33 (2022) 1011–1016

Contents lists available at ScienceDirect

Chinese Chemical Letters

journal homepage: www.elsevier.com/locate/cclet

Flexible, high sensitive and radiation-resistant pressure-sensing hydrogel

Zhiwen Jiang[a], Yusong Wang[b], Guoqing Xu[a], Zhuoni Jiang[a], Zhiqing Ge[a], Mozhen Wang[a,*], Xuewu Ge[a,*]

[a] CAS Key Laboratory of Soft Matter Chemistry, Department of Polymer Science and Engineering, University of Science and Technology of China, Hefei 230026, China
[b] Hefei National Laboratory for Physical Sciences at the Microscale, University of Science and Technology of China, Hefei 230026, China

ARTICLE INFO

Article history:
Received 14 April 2021
Revised 8 June 2021
Accepted 15 June 2021
Available online 22 June 2021

Keywords:
Pressure-sensitive hydrogel
Polyacrylamide
Radiation resistance
Boron nitride nanosheet
Tannic acid
Motion detection

ABSTRACT

Excellent radiation resistance is a prerequisite for pressure-sensitive hydrogels to be used in high-energy radiation environments. In this work, tannic acid-modified boron nitride nanosheet (BNNS-TA) is first prepared as the radiation-resistant additive by a facile one-step ball milling of hexagonal boron nitride and tannic acid. Then, polyacrylamide (PAAm)-based pressure-sensitive hydrogel doped with BNNS-TA and Fe^{3+} ions is fabricated. The ternary BNNS-TA/Fe^{3+}/PAAm hydrogel exhibits excellent compressive strength (at least four times the compressive strength of unfilled pure PAAm hydrogel), pressure-sensitive performance (gauge factor is up to 1.4), and performance recovery due to the combination of multiple intermolecular interactions, such as covalent crosslinking, hydrogen bonds, and ion coordination interactions. The BNNS-TA/Fe^{3+}/PAAm hydrogel can be made as a pressure sensor installed in the control circuit or attached on the human body to detect human activities accurately. More importantly, the compressive strength and the pressure-sensitive performance of the BNNS-TA/Fe^{3+}/PAAm hydrogel can be maintained after the hydrogel is irradiated by ^{60}Co gamma-ray at an absorbed dose of 15 kGy. As a comparison, the compressive strength of the unfilled PAAm hydrogel is only a quarter of that before irradiation. This work not only reveals a facile method to achieve the preparation of chemically modified BNNS as a promising radiation-resistant additive but also provides a novel strategy for the development of pressure-sensitive hydrogel devices in radiation environments.

The conductive hydrogels composed of polymer hydrogels doped with various conductive materials not only have excellent flexibility and high deformability but also have the ability to convert external pressure stimuli into electrical signals sensitively [1-4]. They are considered to be the most promising material for flexible wearable pressure or strain sensors, which can be widely applied in the behavior monitoring of soft robots and human body motion detection [5-8]. With the continuous development of the civil nuclear industry and aerospace technology, pressure-sensitive hydrogels applied in the field of robot operations in the nuclear industry and the astronauts' motion perception in the extravehicular activities are exposed to the high-energy radiation field additionally [9-11]. On the one hand, the polymer components are prone to undergo cross-linking or chain-scission degradation under high-energy radiation [12-16]. On the other hand, $HO^{\bullet}$, $H^{\bullet}$ and other reactive species generated by the γ-ray radiolysis of water will also induce various reactions of polymer chains [17-20]. These radiation chemistry effects will make the hydrogel sensors fail quickly in a high-energy radiation environment [11,20]. Therefore, excellent radiation resistance is a prerequisite for the pressure-sensitive hydrogel sensors to be used in the high-energy radiation field.

There are two ways to improve the radiation resistance of hydrogel materials. One is to design and synthesize new polymers with intrinsic radiation resistance. Generally, the polymer molecular chains containing benzene and other conjugated structure groups exhibit excellent radiation stability [21-23], such as polyether ether ketone (PEEK) [24], polystyrene (PS) [25], polyethylene terephthalate (PET) [26]. However, these kinds of polymers are strongly hydrophobic, which is difficult to be applied to prepare hydrogels. The other way is to add specific fillers that can reduce or suppress the undesirable radiation chemistry effects into the matrix [27-29], such as graphene and hexagonal boron nitride (h-BN). Graphene is usually difficult to prepare. Since there are many active oxygen-containing functional groups on the sur-

* Corresponding authors.
E-mail addresses: pstwmz@ustc.edu.cn (M. Wang), xwge@ustc.edu.cn (X. Ge).

https://doi.org/10.1016/j.cclet.2021.06.043
1001-8417/

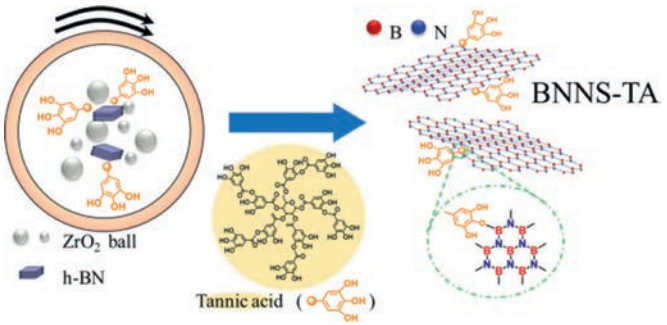

Scheme 1. One-step preparation of BNNS-TA by ball milling with h-BN particles and tannic acid crystals.

face of GO, reduction and hydroxyalkylation reactions induced by the attack of the alcohol free radicals produced by the radiolysis of alcohol/water solution under γ-ray radiation can take place simultaneously on the surface of GO nanosheets, which means GO nanosheets may have enough activity to react with polymer matrix under γ-ray radiation in our previous work [30,31]. By contrast, h-BN has been found to have excellent radiation stability at similar radiation conditions due to its excellent chemical, thermal stability [32-35], and good neutron absorption performance [36-40]. Özdemir *et al*. [37] discovered that h-BN filled silicone composite rubber is a suitable material for neutron shielding purposes, and the attenuation rate (I/I_0) of 60.7% could be achieved for a 6.9 mm thick composite rubber containing 30 wt% of h-BN. In our previous work [39], it is also found that when h-BN is added into the epoxy resin at a mass fraction of more than 0.52%, the composite shows excellent γ-ray radiation resistance. However, h-BN has a poor dispersibility in polymer matrix or water, and the chemical modification of h-BN is also very difficult due to its inherent chemical inertness. These limit the application of h-BN in the preparation of composite materials.

In this work, a tannic acid-assisted ball milling method was first put forward to prepare tannic acid-modified BNNS (BNNS-TA) in one step. The prepared BNNS-TA can be well dispersed in the aqueous solution of acrylamide (AAm) and *N,N*'-methylenebis(acrylamide) (MBA) to fabricate a binary BNNS-TA/PAAm hydrogel. After soaking the binary hydrogel in Fe^{3+} ions aqueous solution, a novel ternary BNNS-TA/Fe^{3+}/PAAM composite hydrogel was prepared.

Tannic acid molecules contain abundant hydroxyl groups, which have strong interactions with PAAm and water molecules. In order to improve the dispersibility of h-BN particles in PAAm hydrogel, we first ball milled the micron-sized h-BN particles and tannic acid crystals together in 300 rpm for 10 h to appropriately reduce the size of h-BN particles and modify them, and obtained tannic-acid modified BNNS (BNNS-TA) in one step, as illustrated in Scheme 1.

The micron-sized raw h-BN particles have a laminated structure formed of stacked thick plates (Fig. S1a in Supporting information). However, BNNS-TA obtained by the ball milling method is in sheet form with a square size of about 200 nm to 300 nm, as shown in Fig. 1a. The actual size of the prepared BNNS-TA can be measured by AFM (Fig. 1b), and more than 91% of BNNS-TA has a thickness of less than 2 nm and a horizontal length of 100~ 200 nm (Figs. S1b and c in Supporting information). XRD spectra (Fig. 1c) display that the crystal structure of BNNS-TA is identical to that of the raw h-BN. The peaks at 2θ of 26.8°, 41.6°, 43.9°, 50.2°, and 55.1° respond to the (002), (100), (101), (102), and (004) planes of h-BN, respectively, according to JCPDS card No. 34–0421, but all diffraction peaks of BNNS-TA become weaker and wider than those of the raw h-BN, indicating the ball milling of h-BN can reduce the particle size, but will not change the crystal structure.

The FT-IR spectrum of BNNS-TA is displayed in Fig. S1d (Supporting information), the absorption peaks at 1726 cm^{-1} and 1203~1038 cm^{-1} assigned to the stretching vibrations of C=O and C–O respectively. Meantime, the UV absorption spectrum of BNNS-TA providing further evidence of the combination between tannic acid molecules and BNNS (Fig. S1e in Supporting information). The thermogravimetric (TG) curves of the raw h-BN and BNNS-TA indicated that the mass loss of 5.42% occurring in the range of 210 ~ 700 °C should be the decomposition of tannic acid in BNNS-TA (Fig. S1f in Supporting information). 2D solid-state ^{11}B MQ MAS NMR spectrum of BNNS-TA was performed in order to determine the interaction between tannic acid molecules and BNNS. It is difficult to accurately distinguish some special chemical environments of ^{11}B by 1D MAS NMR spectrum due to the highly anisotropic interaction of the nuclear quadrupole moment with the gradient of the surrounding electric field [41,42]. As shown in Figs. 1d and e, the 1D solid-state ^{11}B MAS NMR spectra of the raw h-BN and BNNS-TA are almost indistinguishable. However, some overlapped signals of ^{11}B can be effectively discriminated in the projection along F1 dimension in 2D solid-state ^{11}B MQ MAS NMR spectra. Compared with raw h-BN, a new signal of boron atom arises at 20–25 ppm in the spectrum of BNNS-TA (Figs. 1f and g), which means the chemical environment of some B atoms in BNNS-TA has been changed. According to the 2D NMR spectrum of B_2O_3 and the previous report of edge-hydroxylated boron nitride, the new signal should be assigned to the boron acid ester bond (B-O-R) [43,44], indicating that tannic acid molecules have been covalently bonded on the surface of BNNS. Based on the reported theoretical calculations and experimental results [45,46], it is generally recognized that large thick h-BN flakes are fractured and peeled into small thin nanosheets with active B edges during the ball milling. The active B sites at the edges of BNNS tend to react with the -OH groups of tannic acid, resulting in the chemical immobilization of tannic acid on the surface of BNNS [47]. Summarized the above analysis, tannic acid-assisted ball milling can successfully achieve the exfoliation preparation and functionalization of h-BN simultaneously in one step.

After the preparation of BNNS-TA, the fabrication of ternary BNNS-TA/Fe^{3+}/PAAm hydrogel is shown in Fig. 2. BNNS-TA can be dispersed in water homogeneously and stably due to its nano-size and the hydrophilic tannic acid moieties on the surface. They won't precipitate out of water even if left for 14 days, while h-BN particles and the ball-milled BNNS precipitate after standing and it is difficult for the preparation of homogeneous BNNS/Fe^{3+}/PAAm hydrogel samples (Fig. S2 in Supporting information). After the polymerization and crosslinking reactions of AAm and MBA were initiated with ammonium persulfate at 60 °C for 4 h, binary BNNS-TA/PAAm hydrogel was obtained. Then, the binary hydrogel was immersed in the Fe^{3+} ions aqueous solution for 12 h so that Fe^{3+} ions can diffuse into the hydrogel, resulting in the formation of the ternary BNNS-TA/Fe^{3+}/PAAm hydrogel.

The Raman spectra (Fig. S3a in Supporting information) show that three peaks appearing at 409 cm^{-1}, 572 cm^{-1} and 655 cm^{-1} of BNNS-TA/Fe^{3+}/PAAm hydrogel should be assigned to the absorption of tannic acid molecules, and two peaks at 572 cm^{-1} and 655 cm^{-1} should be originated from the vibration of Fe-O [48,49]. This means Fe^{3+} ions in BNNS-TA/Fe^{3+}/PAAm hydrogel are coordinated with -OH groups of TA moieties on BNNS instead of Cl^- ions because the Raman shift of $[FeCl_4]^-$ should be located at 313 nm (Fig. S3b in Supporting information) [50]. Meantime, the UV–vis spectrum of BNNS-TA/Fe^{3+}/PAAm hydrogel in Fig. S3c (Supporting information) shows a broad absorption in the range of 300–500 nm, but PAAm hydrogel and TA molecules have no obvious absorption in this range, which attribute to the redshift of the peak of hydroxyl groups caused by coordination structure. The above analysis demonstrates that the molecular interactions

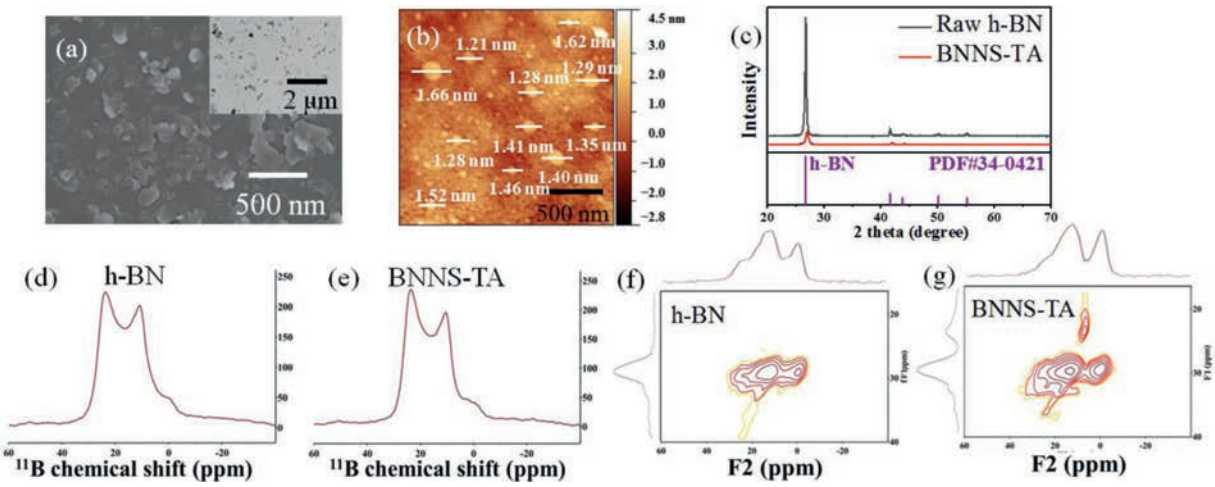

Fig. 1. (a) SEM and TEM (inset) images, and (b) AFM images of the BNNS-TA. (c) XRD diagrams, (d, e) solid-state ^{11}B MAS NMR spectra and (f, g) 2D solid-state ^{11}B MQ MAS NMR spectra of raw h-BN and BNNS-TA.

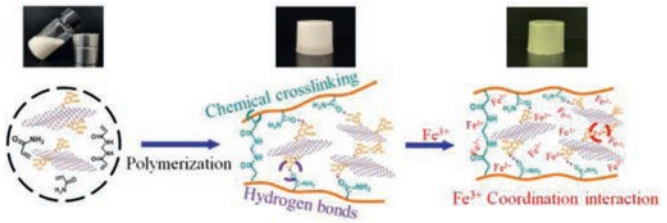

Fig. 2. Preparation and intermolecular interactions of the ternary BNNS-TA/Fe^{3+}/PAAm hydrogel.

in BNNS-TA/Fe^{3+}/PAAm hydrogel include not only the hydrogen bonds formed between hydroxyl groups and water molecules but also the coordination interactions between these phenolic hydroxyl groups and Fe^{3+}.

The compressive stress-strain curves of these hydrogels are shown in Fig. S4a (Supporting information), and the compressive strength and the corresponding strain of pure PAAm hydrogel are 68.1 kPa and 66.9%, respectively. The introduction of BNNS-TA can greatly enhance the compressive strength and flexibility, and the BNNS-TA/PAAm hydrogel will not be broken even when the strain reaches 83.4%, and the corresponding compressive stress is nearly twice that for pure PAAm hydrogel (117.9 kPa), implying a strong affinity between BNNS-TA and polymer chains. However, the compressive modulus of the hydrogel fell with the introduction of BNNS-TA, which indicates that the existence of BNNS-TA may disturb the crosslinking of the polymer chains in the hydrogel, resulting in the decrease of the crosslinking degree. For the ternary BNNS-TA/Fe^{3+}/PAAm hydrogel, it can be seen that the compressive modulus of hydrogel is much higher than the binary hydrogel and the compressive stress increases alarmingly to 217.2 kPa, nearly twice of that for binary BNNS-TA/PAAm hydrogel at a strain of 82.1%. The addition of Fe^{3+} ions enhances the interactions between polymer chains and BNNS-TA through the coordination interactions with hydroxyl groups on BNNS-TA, which is equivalent to increase the crosslinking degree of the polymer chains and resulting in the further improvement of the mechanical property of the composite hydrogel. Moreover, the excellent structure stability of BNNS-TA/Fe^{3+}/PAAm hydrogel is also demonstrated that the compressed hydrogel immediately returns to its original state once the stress is removed (Fig. S4b in Supporting information). The above result shows that Fe^{3+} ions play a key role in enhancing the crosslinking network and strengthening the hydrogel matrix.

Fig. 3a shows that the compressive stress-strain behavior of BNNS-TA/Fe^{3+}/PAAm hydrogel is basically unchanged under the cyclic compression conditions. The corresponding compressive stress retention rates at a certain compression strain (70%) (the ratio of the stress at the n^{th} compression to that at the 1st compression) are also exhibited in Fig. 3b, and demonstrate their outstanding flexibility and recovery mechanical properties. To investigate the influence of the content of Fe^{3+} ions on the mechanical properties, three kinds of BNNS-TA/Fe^{3+}/PAAm hydrogels were prepared by treating the binary BNNS-TA/PAAm hydrogel in the aqueous solution of Fe^{3+} ions with different concentrations (0.2 mol/L, 0.5 mol/L, 1.0 mol/L). Their compressive stress-strain curves over five compression cycles are exhibited in Fig. 3c. Both compressive modulus and strength of the hydrogels are enhanced with the increase of Fe^{3+} concentration, which is consistent with our previous assumption that Fe^{3+} plays a critical part in enhancing the crosslinking network and hydrogel strength.

To evaluate the pressure-sensitive performance of BNNS-TA/Fe^{3+}/PAAm hydrogels, two pieces of copper foils were attached on the top and the bottom of the hydrogels respectively to assemble a pressure sensor. The real-time resistance curves of these hydrogels prepared under different concentrations of Fe^{3+} ions during the compression process are shown in Fig. 3d. The results show that the resistance of hydrogels all changes periodically with the compressive strain. The conductivity of hydrogel obviously increases with the concentration of Fe^{3+}, so the initial resistance of the hydrogels decreases and the range of resistance changes also vary accordingly.

The gauge factors (GF) of BNNS-TA/Fe^{3+}/PAAm hydrogels were calculated to investigate the sensitivity of these pressure-sensitive hydrogels, and their dependence on the strain was plotted in Fig. 3e. Usually, soft or highly compressible conductive materials like hydrogels have a GF lower than 0.8 when they are used as pressure-sensitive elements [51,52]. However, the GF of the prepared BNNS-TA/Fe^{3+}/PAAm hydrogels is greater than 0.8 when the strain is larger than 8.8%. When the strain exceeds 20%, the GF reaches a maximum of 1.4 at a strain of 30.6%, then slows down slightly to 1.1. For comparison, the compressive stress-strain and resistance curves of BNNS-TA/Li^{+}/PAAm hydrogel prepared in the same method are shown in Figs. S4c and d (Supporting information). Although BNNS-TA/Li^{+}/PAAm hydrogel also shows a good compression property, the GF value of the ternary hydrogels containing Fe^{3+} is much higher than that of hydrogels containing Li^{+}, because Li^{+} ions generally have no strong interac-

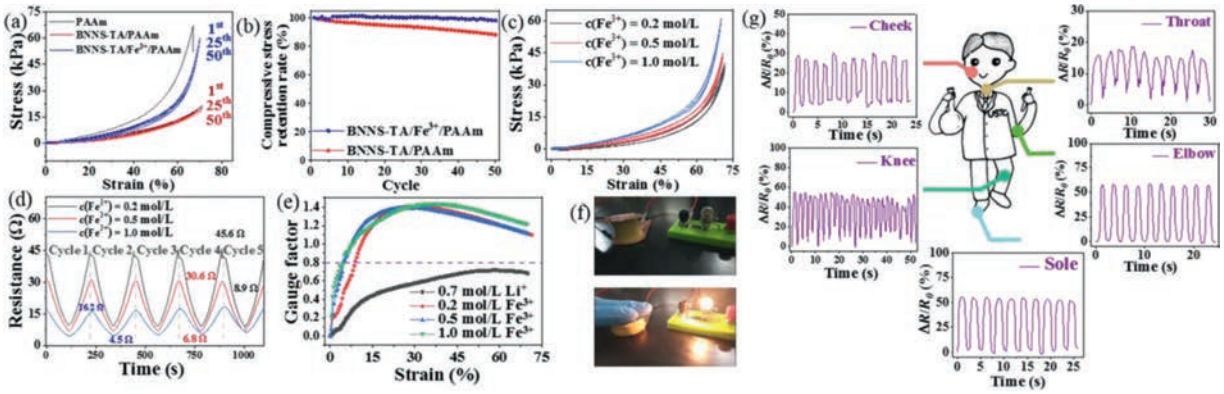

Fig. 3. (a) The compression-relaxation curves at the 1st, 25th and 50th cycle and (b) the compressive stress retention rate curve during 50 cycles at 70% strain of the pure PAAm, BNNS-TA/PAAm and BNNS-TA/Fe^{3+}/PAAm hydrogels. (c) The compression-relaxation curves and (d) the real-time resistance curves of a series of BNNS-TA/Fe^{3+}/PAAm hydrogel. (e) GF *versus* strain for BNNS-TA/Fe^{3+}/PAAm and BNNS-TA/Li^{+}/PAAm. (f) On and off of the bulb can be controlled by the pressure on the hydrogel. (g) Wearable BNNS-TA/Fe^{3+}/PAAm hydrogel sensors applied for human motion detection.

tions with the phenolic hydroxyl groups, leading to worse structure stability of BNNS-TA/Li^{+}/PAAm hydrogel. Interestingly, the GF of BNNS-TA/Fe^{3+}/PAAm hydrogels is closely related to the compressive strain. In a low strain range (< 30%), GF increases sharply with the strain, however, when the strain is large, *e.g.*, > 30%, GF begins to decrease with the strain instead, which can be attributed to the existence of BNNS-TA. Under low strain conditions, BNNS-TA is dispersed scatteredly, Fe^{3+} ions can transport freely in the hydrogel. With the increase of strain, the distance between BNNS-TA nanosheets is gradually reduced, which hinders the directional motion of Fe^{3+} ions and resistance variation, as well as the GF.

BNNS-TA/Fe^{3+}/PAAm hydrogel prepared at a condition of 1.0 mol/L Fe^{3+} ions solution was selected as a representative to investigate the practice performance of BNNS-TA/Fe^{3+}/PAAm hydrogel sensor. First, BNNS-TA/Fe^{3+}/PAAm hydrogel sensor and a small bulb were connected in series in a closed circuit (Fig. 3f). As the deformation magnitude of the hydrogel increased under pressure, the small bulb gradually lit up. As soon as the pressure was removed, the bulb went off. This pressure-induced turn-on-off process of the small bulb could be repeated at will (Video S1 in Supporting information), suggesting that BNNS-TA/Fe^{3+}/PAAm hydrogel can be potentially applied in pressure-sensitive switching elements, pressure-sensing alarm, or 3D bulky pressure sensors. Moreover, the BNNS-TA/Fe^{3+}/PAAm hydrogel was assembled as wearable pressure sensors and attached to five different parts of the human body to detect diverse human activities (Fig. 3g). The sensor can reflect a strong signal to various movements of the human body, including blowing, feeding, and walking, and no obvious shifting of the baseline was observed due to good network structure stability and elasticity of the ternary hydrogel. Furthermore, during the above behavior detection procedure, the prepared sensor as a whole keeps the structure unchanged, and the hydrogel does not fall off or disintegrate, indicating that the BNNS-TA/Fe^{3+}/PAAm hydrogel-based sensor has excellent structural stability. All of these results demonstrate that the BNNS-TA/Fe^{3+}/PAAm hydrogel-based sensor developed in this study has great potential for use in smart devices for the accurate sensing of human motion or robot, and even small deformations can be detected.

The BNNS-TA/Fe^{3+}/PAAm hydrogels were exposed to the ^{60}Co γ-ray radiation field in the air atmosphere at normal temperature and pressure. When the absorbed dose reached 15 kGy (which is equal to the total ionizing dose in 400 km height of an orbits satellite for 20 years [53]), the compressive strength of PAAm hydrogel is 23.0 kPa, only a quarter of original strength (Fig. 4a). While the compressive strength of BNNS-TA/Fe^{3+}/PAAm hydrogel is 84.2 kPa (53.6% of the original strength), basically the same as that of the un-irradiated PAAm hydrogel. It can be seen that the elastic modulus of both the pure PAAm hydrogels and the BNNS-TA/Fe^{3+}/PAAm hydrogel increased (Fig. 4b), which indicates the radiation cross-linking of the PAAm molecular chains is the major radiation chemistry effect [12,28,39]. The compressive stress retention rates show that the compressive stress of BNNS-TA/Fe^{3+}/PAAm hydrogel is basically unchanged after radiation (Fig. 4c), indicating their radiation resistance performance in the mechanical property.

The pressure-sensitive performance of BNNS-TA/Fe^{3+}/PAAm hydrogel after γ-ray radiation shows that the resistance of irradiated ternary hydrogel still changes periodically over 50 compression cycles (Fig. 4d). The resistance of the hydrogel increases with the cycles of compression, which is probably caused by the orientation of BNNS-TA during cyclic compression progress. Meantime, the GF of the sensor after irradiation is slightly declined to 0.9 (Fig. 4e), and the pressure sensor based on BNNS-TA/Fe^{3+}/PAAm hydrogel can still sensitively control the light-on of the bulb in the closed-circuit by repeated compression (Fig. 4f, Video S2 in Supporting information). It proves that BNNS-TA/Fe^{3+}/PAAm hydrogel has excellent radiation resistance in specific high-energy radiation environments.

The radiation resistance is mainly attributed to the following two points: On the one hand, boron nitride has intrinsic structure stability in a radiation environment [36,39]. On the other hand, tannic acid moieties are natural free radical scavengers that can partially remove free radicals, such as $HO^{\bullet}$ and $H^{\bullet}$, generated by the γ-ray radiolysis of water, which can be verified by Fenton-like reaction of Cu^{2+} [54]. The real-time fluorescence emission spectra (λ_{ex} = 315 nm) of the aqueous solution of terephthalic acid (TPA), Cu^{2+}, and H_2O_2 containing BNNS-TA and the raw h-BN at the same content of 5 mg/L were measured (Figs. 4g-i), respectively. TPA can react with $HO^{\bullet}$ radicals to form a hydroxylated product (TPA-OH) which has a strong fluorescence emission at 448 nm. The solution containing BNNS-TA has almost no fluorescence emission signal, but the solution containing h-BN shows strong fluorescence, indicating the existence of TPA-OH. It means BNNS-TA can capture the $HO^{\bullet}$ radicals, but h-BN cannot. The results reveal that BNNS-TA can tremendously reduce the concentration of $HO^{\bullet}$ radicals in the system, thereby reduces the possibility of the attack of free radicals to PAAm molecular chains, so as to slow down the damage to the structure and performance of the hydrogels.

In summary, it is found that tannic acid-assisted ball milling of micron-sized raw h-BN particles can successfully achieve the exfoliation and functionalization of h-BN simultaneously, and obtain nano-sized BNNS-TA in one step. Due to multiple interactions

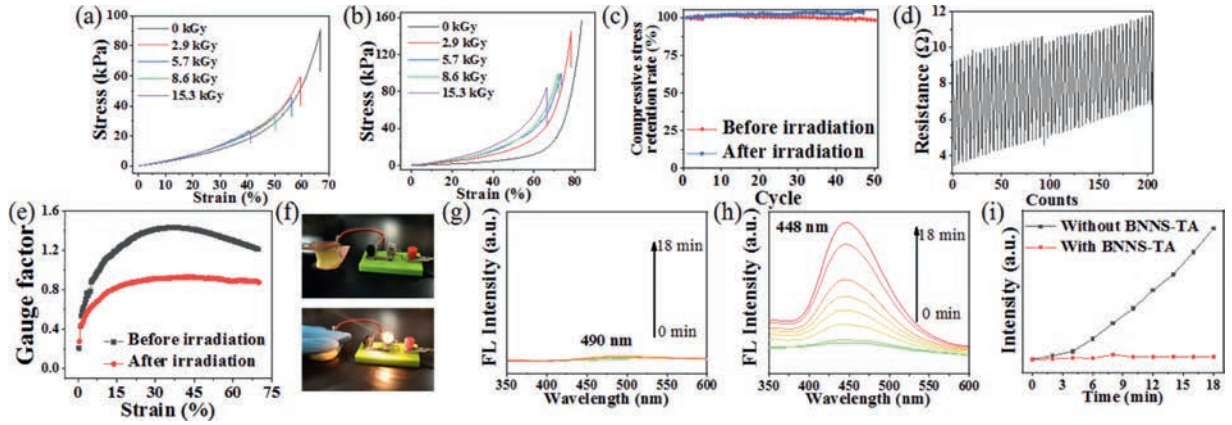

Fig. 4. (a) The compressive stress-strain curves of PAAm hydrogel and (b) BNNS-TA/Fe^{3+}/PAAm hydrogel after ^{60}Co γ-ray irradiation. (c) The compressive stress retention rate curve during 50 cycles of BNNS-TA/PAAm and BNNS-TA/Fe^{3+}/PAAm hydrogel after irradiation. (d) The real-time resistance curves over 50 cycles of irradiated BNNS-TA/Fe^{3+}/PAAm hydrogel. (e) GF *versus* strain for BNNS-TA/Fe^{3+}/PAAm hydrogel before and after irradiation. (f) On and off of the bulb can be controlled by the pressure on the hydrogel. Real-time fluorescence emission spectra (λ_{ex} = 315 nm) of the aqueous solution of $Cu^{2+}$and H_2O_2 containing (g) BNNS-TA and (h) h-BN. (i) The relationship between fluorescence intensity and time derivate from (g) and (h).

including the covalent bond, coordination interaction, and hydrogen bond in the cross-linking network of the hydrogel, the BNNS-TA/Fe^{3+}/PAAm hydrogel exhibits excellent compressive strength (at least four times the compressive strength of unfilled pure PAAm hydrogel), performance recovery (mechanical properties and pressure sensitivity remain after 50 times compression), high sensitivity (gauge factor (GF) is up to 1.4), and can be made as a pressure sensor installed in the control circuit or attached on the human body to detect human activities accurately. More encouragingly, with the help of BNNS-TA as a radical scavenger, the compressive strength and the pressure-sensitive performance of BNNS-TA/Fe^{3+}/PAAm hydrogel can be maintained after the hydrogel is irradiated by ^{60}Co gamma-ray radiation at an absorbed dose of 15 kGy. The results demonstrate that BNNS-TA/Fe^{3+}/PAAm hydrogel has the potential to be applied to prepare the radiation-resistant pressure-sensitive sensor for the safety monitoring and accident handling of nuclear industry production and the extravehicular activities of astronauts. This work provides a novel strategy for the development of pressure-sensitive hydrogel devices in radiation environments.

Declaration of competing interest

The authors declare that they have no known competing financial interests or personal relationships that could have appeared to influence the work reported in this paper.

Acknowledgement

This work was supported by the National Natural Science Foundation of China (Nos. 51773189 and 51973205), the Joint Laboratory for University of Science and Technology of China and Yanchang Petroleum (No. ES2060200084), and the Fundamental Research Funds for the Central Universities (Nos. WK3450000005, WK3450000006).

Supplementary materials

Supplementary material associated with this article can be found, in the online version, at doi:10.1016/j.cclet.2021.06.043.

References

[1] M.A. Darabi, A. Khosrozadeh, R. Mbeleck, et al., Adv. Mater. 29 (2017) 1700533.
[2] G.F. Cai, J.X. Wang, K. Qian, et al., Adv. Sci. 4 (2017) 1600190.
[3] A. Doring, W. Birnbaum, D. Kuckling, et al., Chem. Soc. Rev. 42 (2013) 7391–7420.
[4] R.A. Soomro, S. Jawaid, Q. Zhu, Z. Abbas, B. Xu, Chin. Chem. Lett. 31 (2020) 922–930.
[5] Z.Y. Lei, P.Y. Wu, Nat. Commun. 9 (2018) 1134.
[6] L. He, R. Huang, P. Xiao, et al., Chin. Chem. Lett. 32 (2021) 1593–1602.
[7] Z.Y. Lei, Q.K. Wang, S.T. Sun, W.C. Zhu, P.Y. Wu, Adv. Mater. 29 (2017) 1700321.
[8] M.H. Liao, P.B. Wan, J.R. Wen, et al., Adv. Funct. Mater. 27 (2017) 1703582.
[9] T. Ghidini, Nat. Mater. 17 (2018) 846–850.
[10] C.W. Huang, L. Chen, Adv. Mater. 28 (2016) 8079–8096.
[11] J. Hohe, V. Hardenacke, V. Fascio, et al., Mater. Des. 39 (2012) 20–32.
[12] J. Park, M. Kim, S. Choi, J.Y. Sun, Sci. Rep. 10 (2020) 21689.
[13] M.F. Abou Taleb, H.L.A. El-Mohdy, H.A.A. El-Rehim, J. Hazard. Mater. 168 (1) (2009) 68–75.
[14] X. Jing, H.Y. Mi, X.F. Peng, L.S. Turng, Carbon 136 (2018) 63–72.
[15] R. Galante, C.F. Rediguieri, I.S. Kikuchi, et al., PLoS One 11 (2016) e0168862.
[16] A. Srinivas, A. Ramamurthi, Tissue Eng. 13 (2007) 447–459.
[17] J.L. Marignier, J. Belloni, M.O. Delcourt, J.P. Chevalier, Nature 317 (1985) 344–345.
[18] W.X. Yang, Z.Q. Ge, G.Q. Xu, et al., Appl. Surf. Sci. 531 (2020) 147333.
[19] Z.W. Jiang, W.G. Zhu, G.Q. Xu, et al., J. Mater. Chem. A 8 (2020) 9109–9120.
[20] F.X. Lin, K. Zeng, W.X. Yang, et al., Chin. J. Chem. Phys. 30 (2017) 231–238.
[21] C.G. Delides, Radiat. Phys. Chem. 16 (1980) 345–352.
[22] H. Wei, Y.B. Fu, C.Y. Wang, Y.S. Xu, Z.S. Bian, Radiat. Phys. Chem. 64 (2002) 229–233.
[23] S. Diao, K.K. Jin, Z.Z. Yang, et al., Mater. Chem. Phys. 129 (2011) 202–208.
[24] Y. Wu, Y. Cao, Y. Wu, D.C. Li, Materials (Basel) 13 (2020) 2314.
[25] A. Mosayebi, S. Malekie, F. Ziaie, J. Instrum. 12 (2017) P05012.
[26] H.H. Aygun, M.H. Alma, Appl. Phys. A: Mater. 126 (2020) 693.
[27] D. Tasis, N. Tagmatarchis, A. Bianco, M. Prato, Chem. Rev. 106 (2006) 1105–1136.
[28] K.L.C. Nielsen, D.J.T. Hill, K.A. Watson, et al., Polym. Degrad. Stabil. 93 (2008) 169–175.
[29] S.K. Ghosh, T.K. Chaki, D. Khastgir, R. Pinto, J. Appl. Polym. Sci. 132 (2015) 42017.
[30] W.K. Wang, Y.H. Wu, Z.W. Jiang, et al., Appl. Surf. Sci. 427 (2018) 1144–1151.
[31] W.K. Wang, Y.H. Wu, Z.W. Jiang, Chin. Chem. Lett. 29 (2018) 931–934.
[32] C.Y. Zhi, Y. Bando, C.C. Tang, Q. Huang, D. Golberg, J. Mater. Chem. 18 (2008) 3900–3908.
[33] A. Pakdel, C.Y. Zhi, Y. Bando, D. Golberg, Mater. Today 15 (2012) 256–265.
[34] Z. Liu, Y.J. Gong, W. Zhou, et al., Nat. Commun. 4 (2013) 2541.
[35] Z.Q. Duan, M. Zhong, F.K. Shi, X.M. Xie, Chin. Chem. Lett. 27 (2016) 1490–1494.
[36] J.H. Kang, G. Sauti, C. Park, et al., ACS Nano 9 (2015) 11942–11950.
[37] T. Ozdemir, S.N. Yilmaz, Radiat. Phys. Chem. 152 (2018) 93–99.
[38] F. Cataldo, M. Prata, J. Radioanal. Nucl. Chem. 320 (2019) 831–839.
[39] W.G. Zhu, Z.W. Jiang, H.B. Chen, et al., J. Radiat. Res. Radiat. Process. 38 (2020) 10–20.
[40] C. Harrison, S. Weaver, C. Bertelsen, et al., J. Appl. Polym. Sci. 109 (2008) 2529–2538.
[41] C. Gervais, J. Maquet, F. Babonneau, et al., Chem. Mater. 13 (2001) 1700–1707.
[42] B. Qiu, F. Jiang, W.D. Lu, et al., J. Catal. 385 (2020) 176–182.
[43] A.M. Love, B. Thomas, S.E. Specht, et al., J. Am. Chem. Soc. 141 (2019) 182–190.
[44] S.J. Hwang, C. Fernandez, J.P. Amoureux, et al., Solid State Nucl. Magn. Reson. 8 (1997) 109–121.
[45] S.H. Chen, R.Z. Xu, J.M. Liu, et al., Adv. Mater. 31 (2019) 1804810.
[46] H. Shalchian, J.V. Khaki, A. Babakhani, et al., Ceram. Int. 43 (2017) 12957–12967.
[47] W.W. Lei, V.N. Mochalin, D. Liu, et al., Nat. Commun. 6 (2015) 8849.

[48] M.J. Harrington, A. Masic, N. Holten-Andersen, J.H. Waite, P. Fratzl, Science 328 (2010) 216–220.
[49] N. Holten-Andersen, M.J. Harrington, H. Birkedal, et al., Proc. Natl. Acad. Sci. USA 108 (2011) 2651–2655.
[50] J.S. Avery, C.D. Burbridge, D.M. Goodgame, Spectroc. Acta Pt. A: Molec. Biomolec. Spectr. 24 (1968) 1721–1726.
[51] X.H. Zhang, N.N. Sheng, L.A. Wang, et al., Mater. Horizons. 6 (2019) 326–333.
[52] Z.X. Deng, Y. Guo, X. Zhao, P.X. Ma, B.L. Guo, Chem. Mater. 30 (2018) 1729–1742.
[53] J. Zimmermann, M.Z. Sadeghi, K.U. Schroeder, Int. J. Adhes. Adhes. 93 (2019) 102334.
[54] Z. Shan, M.S. Lu, L. Wang, et al., Chem. Commun. 52 (2016) 2087–2090.